

Search for Θ^+ via $K^+p \rightarrow \pi^+X$ reaction with a 1.2 GeV/c K^+ beam

K. Miwa,^{1,*} S. Dairaku,¹ D. Nakajima,² S. Ajimura,^{3,†} J. Arvieux,⁴ H. Fujimura,¹ H. Fujioka,² T. Fukuda,⁵ H. Funahashi,^{1,‡} M. Hayata,¹ K. Hicks,⁶ K. Imai,¹ S. Ishimoto,⁷ T. Kameyama,⁸ S. Kamigaito,¹ S. Kinoshita,⁹ T. Koike,⁹ Y. Ma,⁹ T. Maruta,^{2,§} Y. Miura,⁹ M. Miyabe,¹ T. Nagae,^{7,¶} T. Nakano,¹⁰ K. Nakazawa,⁸ M. Naruki,^{11,**} H. Noumi,^{7,†} M. Niiyama,^{1,††} N. Saito,^{1,‡‡} Y. Sato,⁷ S. Sawada,⁷ Y. Seki,¹ M. Sekimoto,⁷ K. Senzaka,¹ K. Shirotori,⁹ K. Shoji,¹ S. Suzuki,⁷ H. Takahashi,⁷ T. Takahashi,⁷ T.N. Takahashi,² H. Tamura,⁹ N. Tanaka,⁷ K. Tanida,^{11,¶} A. Toyada,⁷ T. Watanabe,⁸ M. Yosoi,¹⁰ and R. Zavislak⁶

¹Department of Physics, Kyoto University, Kyoto 606-8502, Japan

²Department of Physics, University of Tokyo, 7-3-1 Hongo, Tokyo 113-0033, Japan

³Department of Physics, Osaka University, Toyonaka 560-0043, Japan

⁴Institut de Physique Nucléaire, Université Paris Sud, F-91406 Orsay cedex, France

⁵Department of Physics, Osaka Electric Communication University, Osaka 558-8585, Japan

⁶Department of Physics, Ohio University, Athens, Ohio, USA 45701

⁷KEK, High Energy Accelerator Research Organization, Tsukuba 305-0801, Japan

⁸Physics Department, Gifu University, Gifu 501-1193, Japan

⁹Department of Physics, Tohoku University, Sendai 980-8578, Japan

¹⁰Research Center for Nuclear Physics (RCNP), 10-1 Mihogaoka, Ibaraki, Osaka, 567-0047, Japan

¹¹RIKEN, 2-1 Hirosawa, Wako, Saitama 351-0198, Japan

(Dated: August 15, 2019)

The Θ^+ was searched for via the $K^+p \rightarrow \pi^+X$ reaction using the 1.2 GeV/c K^+ beam at the K6 beam line of the KEK-PS 12 GeV Proton Synchrotron. In the missing mass spectrum of the $K^+p \rightarrow \pi^+X$ reaction, no clear peak structure was observed. Therefore a 90 % C.L. upper limit of 3.5 $\mu\text{b}/\text{sr}$ was derived for the differential cross section averaged over 2° to 22° in the laboratory frame of the $K^+p \rightarrow \pi^+\Theta^+$ reaction. This upper limit is much smaller than the theoretical calculation for the t -channel process where a K^{0*} is exchanged. From the present result, either the t -channel process is excluded or the coupling constant of $g_{K^*N\Theta}$ is quite small.

PACS numbers: 12.39.Mk, 13.75.Jz, 14.20.-c

I. INTRODUCTION

Since the first report giving evidence of the existence of an exotic baryon Θ^+ [1], many papers from both theoretical and experimental aspects have been published [2, 3]. The Θ^+ was observed as a narrow resonance of a K^+n system, giving its minimum quark content as $uudd\bar{s}$. Therefore, if the Θ^+ would exist, it could have interesting consequences for non-perturbative QCD. The first observation by the LEPS collaboration was confirmed by several experiments [4, 5, 6, 7, 8, 9, 10, 11, 12, 13]. How-

ever, null results were also reported from several high energy experiments where they searched for the Θ^+ with much higher statistics [14, 15, 16, 17, 18, 19, 20]. Moreover, some of the initial positive evidence was refuted by the same collaboration with higher statistics [22, 23, 24]. On the other hand, the LEPS and DIANA collaborations have shown new evidence supporting its existence. The LEPS collaboration shows a narrow peak in the missing mass spectrum of the $\gamma d \rightarrow \Lambda(1520)X$ reaction [25]. The DIANA collaboration confirmed its initial positive evidence with two times larger statistics [26]. In this controversial situation, it is quite important to perform other experimental searches that would reveal the production mechanism of the Θ^+ by using various reactions.

If the Θ^+ exists, one of its most remarkable features would be its narrow width. The observed width is consistent with the experimental resolution in all positive experiments. Moreover reanalyses of the past K^+ -nucleon elastic scattering restricted the width to be less than a few MeV/c^2 [27]. Cahn and Trilling calculated the width from the result of the DIANA experiment, where the Θ^+ was observed via the charge exchange channel of $K^+n \rightarrow K^0p$, and obtained the width of $0.9 \pm 0.3 \text{ MeV}/c^2$ [28]. Such narrow width is unusual for a hadron resonance. In order to understand the narrow width, theoretical models were proposed that take into account an additional correlation between quarks [29, 30, 31, 32, 33, 34]. The different dynamics of several models results in different

*Corresponding author, email: miwa9@lambda.phys.tohoku.ac.jp, Present address: Department of Physics, Tohoku University, Sendai 980-8578, Japan

†Present address: Research Center for Nuclear Physics (RCNP), 10-1 Mihogaoka, Ibaraki, Osaka, 567-0047, Japan

‡Present address: Department of Physics, Osaka Electric Communication University, Osaka 558-8585, Japan

§Present address: Department of Physics, Tohoku University, Sendai 980-8578, Japan

¶Present address: Department of Physics, Kyoto University, Kyoto 606-8502, Japan

**Present address: KEK, High Energy Accelerator Research Organization, Tsukuba 305-0801, Japan

††Present address: RIKEN, 2-1 Hirosawa, Wako, Saitama 351-0198, Japan

‡‡Present address: Present address: KEK, High Energy Accelerator Research Organization, Tsukuba 305-0801, Japan

values of the spin and parity. Therefore experimentally, if the Θ^+ exists, it is quite important to determine its spin and parity to understand the nature of the Θ^+ and hence its quark dynamics. For this purpose, experiments with high statistics are needed. Hadronic reactions fulfill these requirements, because the production cross section via a hadronic reaction is expected to be much larger than that of a photoproduction reaction. Theoretically, the cross section of the $K^+p \rightarrow \pi^+\Theta^+$ reaction is expected to be $\sim 80\mu\text{b}$ [35].

High-resolution spectroscopy is another important point. Because the width of the Θ^+ is expected to be narrow, high resolution is essential in order to measure its width with high experimental sensitivity. Therefore we were motivated to do an experiment using a K^+ beam and a high resolution spectrometer to search for the Θ^+ with high statistics.

A different experiment, the E522 collaboration, reported a search for the Θ^+ via the $\pi^-p \rightarrow K^-X$ reaction [36], finding a bump structure near $1.53\text{ GeV}/c^2$ in the missing mass spectrum off the K^- . The statistical significance of the bump was $2.5 - 2.7\sigma$ and was not sufficient to claim the existence of the Θ^+ . The upper limit of the production cross section was found to be $3.9\mu\text{b}$. This reaction is just the inverse reaction of $K^+p \rightarrow \pi^+X$. In both reactions, the same coupling constants are used in the production diagrams. A deeper understanding on the production mechanism can be obtained by considering both experimental results.

Theoretical calculations in hadronic models using effective interaction Lagrangians and form factors were made by several authors [35, 42, 43, 44, 45]. They studied the Θ^+ production mechanism in $\gamma N, NN, KN$ and πN reactions near the production threshold comprehensively. In general all calculations predict a large production cross section for the $K^+p \rightarrow \pi^+\Theta^+$ reaction. For the production process, they took into account both the t-channel process, where K^{0*} was exchanged, and the u-channel process, which includes intermediate N^* states. In these calculations, unknown coupling constants, $g_{KN\Theta}$ and $g_{K^*N\Theta}$ were used. Therefore measurements of both $K^+p \rightarrow \pi^+\Theta^+$ and $\pi^-p \rightarrow K^-\Theta^+$ reactions are useful to compare with theory.

In this paper, we show the results of a search for the Θ^+ via the $K^+p \rightarrow \pi^+X$ reaction. We discuss the production mechanism considering both experimental results of $K^+p \rightarrow \pi^+\Theta^+$ and $\pi^-p \rightarrow K^-\Theta^+$ reactions.

II. EXPERIMENT

In order to search for the Θ^+ via the $K^+p \rightarrow \pi^+\Theta^+$ reaction using a high-resolution spectrometer called SKS [37], an experiment has been performed at the K6 beam line of the KEK 12 GeV proton synchrotron (KEK-PS E559). Data were taken in two separated periods; one month in June 2005 (1st run) and two weeks in December 2005 (2nd run). We searched for the Θ^+ using the

missing mass technique by detecting incident K^+ beam particles and an outgoing π^+ using the K6 beam line spectrometer and the SKS spectrometer, respectively. Originally, the K6 beam line and SKS spectrometer were constructed for high-resolution spectroscopy of Λ hypernuclei using high intensity π^+ beam particles [38, 39]. The advantage of the present experiment is the excellent mass resolution of $2.4\text{ MeV}/c^2$ (FWHM) which is comparable to the expected width of the Θ^+ . In this reaction, a large background is present, which originates from Δ and K^* productions with cross section of $\sim 5\text{mb}$ [40], in addition to decays of the incident K^+ beam. The SKS provides good mass resolution leading to high sensitivity. The experimental setups of the K6 beam line and SKS spectrometers are shown in Fig. 1 and 2.

In the present experiment, for the first time a K^+ beam was used in this beam line. The central momentum of the K^+ beam was set to $1.2\text{ GeV}/c$, which was the maximum momentum of the K6 beam line. The K6 beam line supplied various mass-separated secondary beams using an electrostatic separator with two correction magnets. The K^+/π^+ ratio in the beam was about 0.1. The incident particle was defined by two hodoscopes (BH1, BH2) placed about 9 m apart. Protons in the beam were rejected at the trigger level using a time difference of 7 ns between protons and K^+ 's. In order to reject beam π^+ 's in the online trigger, an Aerogel Cherenkov counter (BAC), whose index of refraction was 1.06, was installed just upstream of a liquid hydrogen target system. The efficiency was $98.7\pm 0.1\%$ for $1.2\text{ GeV}/c$ π^+ 's, while the overkill rate for K^+ 's was $3.0\pm 0.2\%$. Each incident particle was analysed with the K6 beam line spectrometer which consisted of a QQDQQ magnet system and drift chambers (BDC1.2.3.4) located upstream and downstream of these magnets. The bending angle was 60 degree. The expected momentum resolution was $\Delta p/p=0.047\%$ (FWHM).

A newly developed liquid hydrogen target had a cooling system using a liquid helium. The hydrogen vessel was made from PET (Polyethylene Terephthalate) for the cylinder, and Mylar for the end caps. The target was 6.87 cm in diameter and 12.5 cm in length. During the experimental period, the volume and pressure of the target were monitored and fluctuated less than 1%.

The scattered π^+ 's were detected with the SKS spectrometer located at forward angles. The magnetic field was 1.6 T, where the momentum of the central trajectory was $0.52\text{ GeV}/c$. The SKS covered the angular region smaller than 25° and had an acceptance in the laboratory frame of $\sim 0.11\text{ sr}$ for particles whose momentum was $0.46 - 0.60\text{ GeV}/c$. The momentum of each outgoing particle was analysed with four drift chambers (SDC1.2.3.4) located upstream and downstream of the SKS magnet. The momentum resolution was estimated to be $\Delta p/p=0.42\%$ (FWHM) from the difference of momenta analysed by both spectrometers for beam-through events. For particle identification, trigger counters (TOF, AC1.2, LC) were placed downstream of SDC4. Both

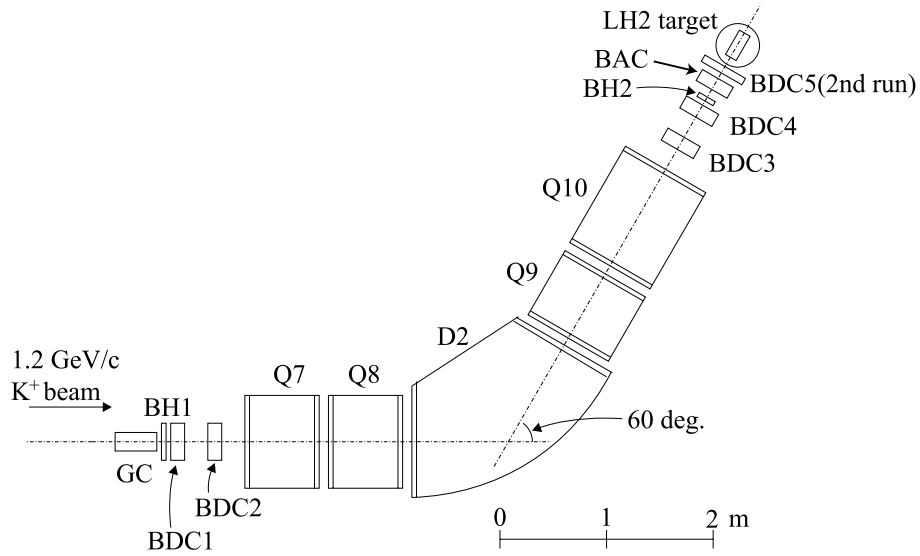


FIG. 1: Experimental setup of the K6 beam line spectrometer.

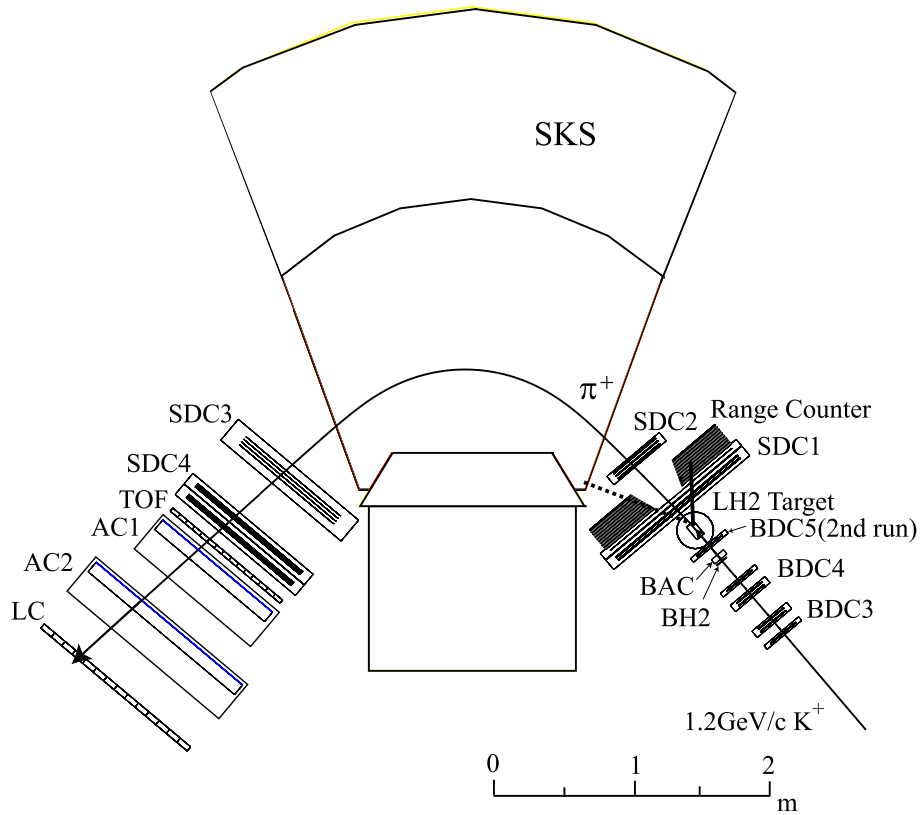


FIG. 2: Experimental setup of the SKS spectrometer. The SDC1 and a Range Counter (RC) were newly installed in order to detect the charged particles other than a π^+ detected with SKS. The BDC5 was used only in the 2nd run to reject reaction events at BAC and BH2.

TOF and LC hits were required to select a π^+ in the online trigger. Outgoing protons were rejected using LC. The LC efficiency was typically 95% for π^+ 's. In offline analysis, the mass was reconstructed from the momentum and the time-of-flight between BH2 and TOF.

In order to suppress background events, we modified the detector setup around the target as shown in Fig. 2. For background events, there are hadronic reactions such as $K^+p \rightarrow \Delta K \rightarrow \pi^+KN$ and $K^+p \rightarrow NK^* \rightarrow \pi^+KN$. The total cross section of each reaction has been mea-

TABLE I: Summary of the obtained data

Reaction	Beam	Target	Number of beam (1st)	Number of beam (2nd)
(K^+, π^+)	1.2GeV/c K^+	LH ₂	3.31×10^9	2.17×10^9
(π^+, π^+)	1.2GeV/c π^+	LH ₂		
(K^+, π^+)	1.2GeV/c K^+	empty	2.35×10^8	3.87×10^8
(π^+, K^+)	1.1GeV/c π^+	LH ₂	8.67×10^9	1.71×10^9

sured to be 3.75 ± 0.32 mb and 1.06 ± 0.20 mb, respectively [40]. However, the most serious background came from decay events of K^+ beam particles. Although the kinematical distribution of these two-body decays was out of the SKS acceptance, three-body decays ($K^+ \rightarrow \pi^+\pi^+\pi^-$, $\pi^+\pi^0\pi^0$, $\mu^+\pi^0\nu_\mu$ and $e^+\pi^0\nu_e$) could be a large background which was ten times larger than that from hadronic reactions. Therefore the rejection of these decay events was crucial in the search for the Θ^+ . The decay events were separated from the reaction events using the difference of the angular distribution and the number of charged particles emitted in each event. For the three-body decays of the K^+ , one or three charged particles were emitted in the forward angle within 20° , whereas two or four charged particles were emitted in the hadronic reaction events with final states π^+K^+n or π^+K^0p . When a π^+ was detected by the SKS, other charged particles were emitted at large angles (0 - 100 degrees for a K^+ and 0 - 50 degrees for a proton). Therefore, in order to detect all possible charged particles and measure the angle, a large acceptance drift chamber (SDC1) whose effective area was 1200mm \times 1200mm was installed just downstream of the LH₂ target. The SDC1 covered from 0 to 60 degrees. The SDC1 consisted of five planes (X,X',Y,Y',U). The maximum drift lengths were 4.5mm and 9.0mm for X, X', Y and Y' planes and U plane, respectively. The SDC1 measured the angle using hit information and vertex position obtained from trajectories of the K^+ and the π^+ . The decay events were suppressed in the offline analysis using SDC1. In order to improve the signal-to-noise S/N ratio to detect an emitted K^+ , a range counter (RC) which had the same effective area with SDC1 was installed just downstream of SDC1. The RC consisted of 10 layers of plastic scintillators and 9 layers of brass absorbers, placed alternately. The thicknesses of the scintillator and the brass absorber were 8mm and 9mm, respectively. Each scintillator layer was segmented horizontally into 5 segments. The light from the scintillator was collected from PMT's attached on the top and bottom ends. In order to avoid the scattering of outgoing π^+ 's detected with SKS from the material of RC, there was a hole at the entrance region to the SKS magnet.

In total, 3.31×10^9 and 2.17×10^9 K^+ beam particles were irradiated in the 1st and 2nd runs, respectively. In addition to (K^+, π^+) events, we took (π^+, π^+) events in order to estimate some of cut efficiencies. The mass scale and resolution were calibrated using a Σ^+ peak produced via the $\pi^+p \rightarrow K^+\Sigma^+$ reaction using a 1.1 GeV/c π^+

beams. The obtained data are summarized in Table I.

III. ANALYSIS & RESULTS

The analysis of beam particles consisted of the identification of K^+ particles and the analysis of the momentum. The incident K^+ beam particles were identified with time-of-flight between BH1 and BH2 as shown in Fig 3. A typical time difference of the π^+ and K^+ was 1.9 ns. The time resolution after a correction using the ADC was $\sigma = 205$ ps. We selected a $\pm 4\sigma$ region to identify K^+ particles. The beam momentum was reconstructed using hit information of the drift chambers and a third order transfer matrix.

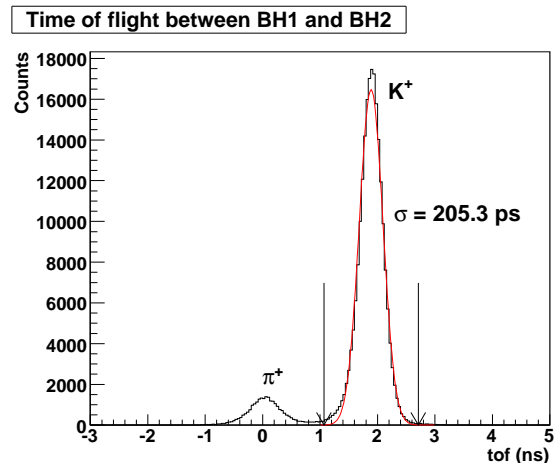


FIG. 3: Time-of-flight distributions between BH1 and BH2. The arrows indicate the selection window for K^+ beam particles which is the $\pm 4\sigma$ region of its time resolution.

The trajectory of each scattered particle was reconstructed from its position in the drift chambers and a field map of the SKS magnet. The straight tracks were defined by fitting locally upstream and downstream of the SKS magnet. These local tracks were connected using the Runge-Kutta method [41]. Tracks of reduced $\chi^2 < 100$ were selected as good tracks. In order to determine the χ^2 limit, the peak width of the Σ^+ was checked for each reduced χ^2 region. The cut position was determined as a region where a reasonable resolution (less than 3.3 MeV/ c^2 (FWHM)) was obtained. From the reconstructed mass distribution, the scattered π^+ 's were

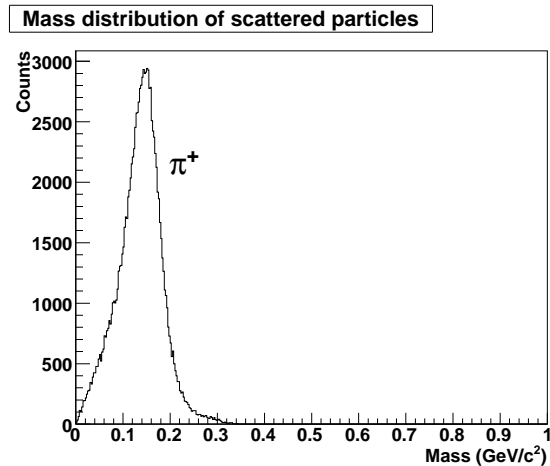


FIG. 4: Distribution of obtained masses of scattered particles.

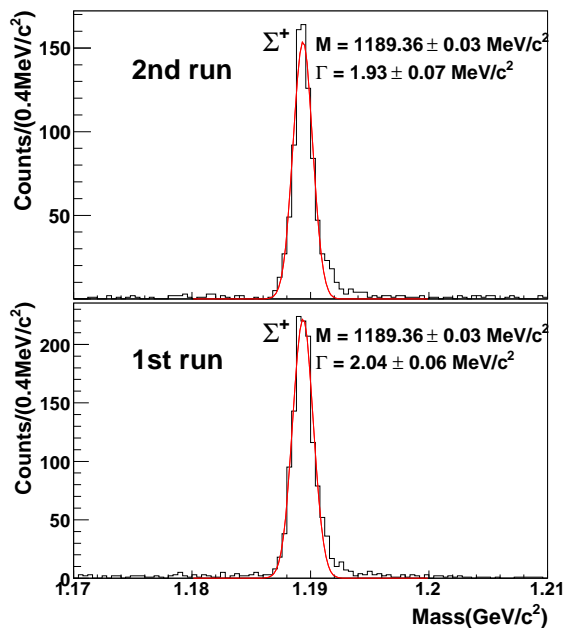


FIG. 5: Missing mass spectra of the $\pi^+p \rightarrow K^+X$ reaction for the 1st and 2nd runs. The peak of Σ^+ is seen. The obtained widths are consistent with the expected value of $1.98 \text{ MeV}/c^2$ obtained from a Monte Carlo simulation. The peak positions for both runs are consistent with each other.

clearly selected as shown in Fig. 4.

The validity of the analyses of both spectrometers was confirmed using the $\pi^+p \rightarrow K^+\Sigma^+$ reaction taken for calibration with a $1.1 \text{ GeV}/c$ π^+ beam. The missing mass spectra of the $\pi^+p \rightarrow K^+X$ reaction are shown in Fig. 5 for the 1st and 2nd runs, where clear peaks of Σ^+ are identified. The obtained widths for both runs are consistent with the expected value of $1.98 \text{ MeV}/c^2$ from a Monte Carlo simulation considering the momentum

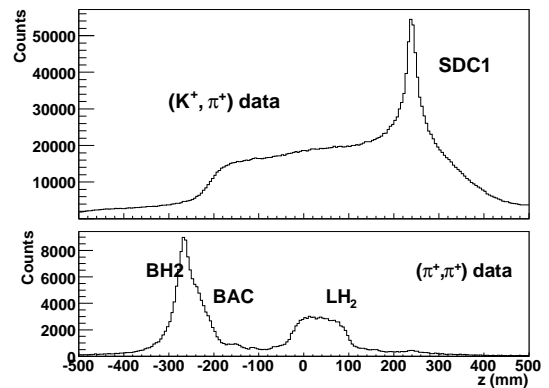


FIG. 6: Vertex distributions of the (K^+, π^+) and (π^+, π^+) data. In the vertex distribution of the (π^+, π^+) data, the image of the LH_2 target as well as BH_2 and BAC is seen. The distribution in the (K^+, π^+) data was flat from BAC position ($z = -220$) because almost all events of the (K^+, π^+) data are decay events. The peak structure around $z = 230 \text{ mm}$ was due to miscalculated events of K^+ beam particles, which decayed between SDC1 and SDC2 .

resolution of $\Delta p/p = 0.047\%$ (FWHM) and $\Delta p/p = 0.43\%$ (FWHM) for the K6 and SKS spectrometers. The absolute value of the momentum of outgoing particle was adjusted to make the Σ^+ peak consistent with its known value. The mass shift from the known value was $1 \text{ MeV}/c^2$ which corresponded to $3 \text{ MeV}/c$ correction of the momentum. This momentum correction corresponds to $2 \text{ MeV}/c^2$ shift for the peak position of the Θ^+ . From Monte Carlo simulations, the missing mass resolution for the Θ^+ was estimated to be $2.4 \text{ MeV}/c^2$ (FWHM). Because the peak positions of the Σ^+ are consistent for the 1st and 2nd runs, the missing mass resolution of the Θ^+ is not expected to decrease by adding the missing mass spectra of the 1st and 2nd runs.

The vertex position was reconstructed at the point of the distance of closest approach between the incident and the scattered tracks. Fig. 6 shows the distribution of the vertex positions of the (K^+, π^+) and (π^+, π^+) data. In the vertex distribution of the (π^+, π^+) data, the image of the LH_2 target, as well as BH_2 and BAC , are clearly seen. On the other hand, in the (K^+, π^+) data, we could not recognize the LH_2 target because almost all events of the (K^+, π^+) data are decay events. The peak structure around $z = 230 \text{ mm}$, which corresponded to the position of SDC1 , was due to miscalculated events of K^+ beam particles that decayed between SDC1 and SDC2 . In order to suppress these decay events, we used information on the number of tracks just after the target and their angles. In order to detect all possible charged particles, a large acceptance chamber (SDC1) was installed. Tracks other than π^+ measured with SKS were reconstructed from the hit information of SDC1 and the 1st layer of RC, and the reconstructed vertex position. Because more than two charged particles were emitted at

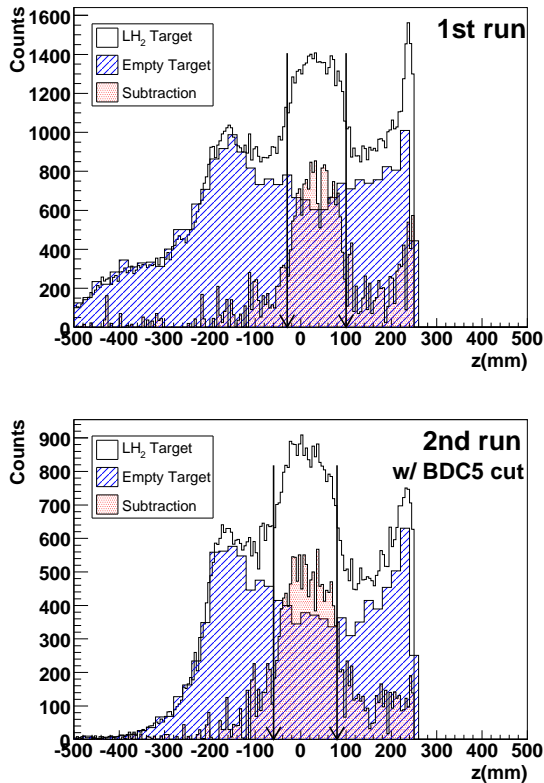


FIG. 7: Vertex distributions of the (K^+, π^+) reaction after the decay suppression using SDC1 for the 1st and 2nd runs. The open histogram shows the vertex distribution obtained using the LH₂ target data. The blue hatched histogram shows the empty target data, which are normalized using the beam flux. The red dotted histogram shows the subtraction of these histograms, which shows a net contribution of the $K^+p \rightarrow \pi^+X$ reaction events. The arrows show the cut position for the vertex cut.

large angles for hadronic reaction, the number of tracks just after the target was required to be more than two. When the number detected by SDC1 was two, i.e. one more particle other than π^+ detected with SKS, the angle of the second particle was required to be larger than 10° . When the number was more than three, the angles of the second and third particles were required to be more than 15° and 23° , respectively. The cut positions of these angles were determined so as to make S/\sqrt{N} a maximum, where S is the number of hadronic reaction events and N is the decay events in the vertex region between the arrows in Fig. 7. Fig. 7 shows the vertex distribution after this analysis of SDC1. The vertex of the LH₂ target was seen once the decay events were removed. The hatched histogram shows the empty target data which is normalized using the beam flux. The dotted spectrum shows the subtraction of histograms of the LH₂ target data and the normalized empty target data. The subtracted spectrum shows the net contribution of the $K^+p \rightarrow \pi^+X$ reaction at the LH₂ target. The number of reaction events are

1.7×10^4 and 1.2×10^4 , respectively, for the 1st and 2nd runs.

Using the analysis of SDC1, 95% of decay events at the target region were removed. As shown in Fig. 7, there are still decay events. One can test whether the amount of decay events is consistent or not by comparing with a Monte Carlo simulation. Based on the Monte Carlo simulation where efficiencies of the chambers were taken into account, the suppression factor for the decay events was estimated to be 98%. The reason of this inefficiency was that one of the pions from three-body decay disappeared by the interaction with the LH₂ target or materials around the target. The e^+e^- from π^0 decay also created mistaken tracks and decreased the efficiency. From this study, we found that there is $\sim 3\%$ difference between the real data and the simulation. To explain this difference, we considered whether the K_S^0 's, which were produced at BH2 or BAC via hadronic reactions such as $K^+n \rightarrow K_S^0p$, could contribute to the vertex distribution, because the K_S^0 's which decayed into $\pi^+\pi^-$ at the target region made a miscalculated vertex at the cross point between the π^+ and the K^+ beam. In the 2nd run, in order to remove these events, a new drift chamber (BDC5) with two planes (X, X') was installed between the target and BAC. We applied the following cuts. At first, the hit position of BDC5 was required to be consistent with the extrapolated position from the track defined with BDC3-4. We also required the multiplicity of BDC5 to be one. The bottom figure in Fig. 7 shows the vertex distribution applied the BDC5 cut in the 2nd run, which shows a slight improvement of the S/N ratio. However there is still about 2% inconsistency between the analysis and the simulation. This could be due to the imperfection of the Monte Carlo simulation, since we could not reproduce the complex LH₂ target system where some materials were not installed. Another possible reason is incompleteness of the analysis of SDC1. We took this 2% inconsistency into account as the systematic error of the efficiency of the SDC1 analysis described in the following paragraph.

The efficiency of the SDC1 analysis for the Θ^+ events was also checked by this Monte Carlo simulation. Because charged particles other than π^+ in SKS were required to be detected by SDC1, the acceptance of the chamber must be considered for these particles and the tracking efficiency of the SDC1 analysis. In this simulation, we assumed the following three kinds of angular distributions of π^+ in the center of mass system;

1. flat distribution,
2. forward peak distribution $((1 + \cos\theta)/2)$,
3. backward peak distribution $((1 - \cos\theta)/2)$,

where θ is the angle of π^+ in the K^+p center of mass (c.m.) system. For the decay distribution of $\Theta^+ \rightarrow KN$, a flat distribution was assumed. The branching ratios of $\Theta^+ \rightarrow K^+n, K_S^0p$ and K_L^0p were assumed to be 50%, 25% and 25%, respectively. Between these distributions,

TABLE II: Summary of the cuts and their efficiencies.

	cut	efficiency(%) (1st run / 2nd run)
f_{K^+beam}	K^+ beam on-target factor	$84.5 \pm 3.5 / 96.2 \pm 1.6$
f_{K^+decay}	K^+ beam decay factor	$96.7 \pm 0.1 / 95.7 \pm 0.1$
ϵ_{K6}	tracking efficiency of beam particle	$95.3 \pm 0.3 / 95.6 \pm 0.3$
ϵ_{LC}	LC efficiency	95.5 ± 0.2
ϵ_{TOF}	TOF efficiency	$\sim 100.$
f_{π^+decay}	π^+ decay factor	85.2 ± 0.2
f_{π^+int}	π^+ interaction factor	94 ± 2
ϵ_{SdcIn}	SdcIn tracking efficiency	87 ± 1
ϵ_{SdcOut}	SdcOut tracking efficiency	92.9 ± 0.3
ϵ_{Sks}	Sks tracking efficiency	95 ± 0.7
ϵ_{Sdc1}	Sdc1 analysis efficiency	69.4 ± 3.7
ϵ_{vtx}	vertex cut efficiency	$85.2^{+2.9}_{-1.3} / 85.0^{+0.4}_{-0.9}$
ϵ_{Bdc5}	BDC5 cut efficiency	$— / 91.6 \pm 0.2$
$d\Omega$	acceptance at lab. frame	$0.11 \text{sr}.$

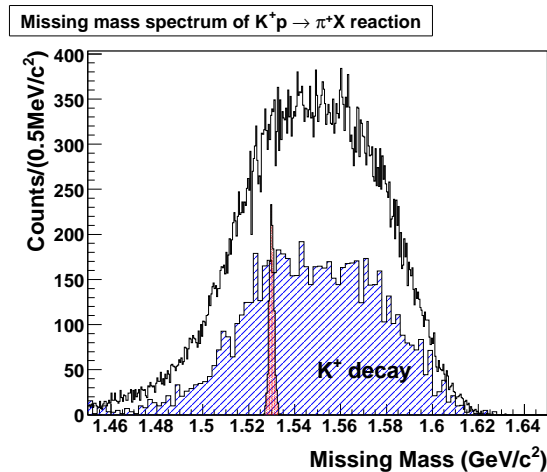


FIG. 8: Missing mass spectrum of the $K^+p \rightarrow \pi^+X$ reaction where the spectra of the 1st and 2nd runs are added. The hatched histogram shows the empty target data, which are normalized using the beam flux. The dotted spectrum shows the expected spectrum assuming that the width of the Θ^+ is 0 MeV/ c^2 , the total cross section of the $K^+p \rightarrow \pi^+\Theta^+$ reaction is $50 \mu\text{b}$ and the angular distribution of the π^+ is isotropic in the K^+p c.m. system.

the difference was small and the efficiency was estimated to be $69.4 \pm 3.7\%$. The error consisted of two parts. The first one is the deviation between the different angular distributions. The other one is the 2% uncertainty of tracking analysis using SDC1 as described in the previous paragraph.

Fig. 8 shows the missing mass spectrum of the $K^+p \rightarrow \pi^+X$ reaction after selecting the LH₂ target regions using the vertex distribution. In this figure, the data of the 1st and 2nd runs are added. The hatched histogram shows the empty target data, which are normalized using the beam flux. This spectrum shows the contribution from the K^+ decays in the region between the arrows in Fig. 7. The dotted spectrum shows the expected spec-

trum assuming that the width of the Θ^+ is 0 MeV/ c^2 , the total cross section of the $K^+p \rightarrow \pi^+\Theta^+$ reaction is $50 \mu\text{b}$ and the angular distribution of the π^+ is isotropic in the K^+p c.m. system. In the present experiment, no significant peak was observed. We also obtained the differential cross section averaged over 2° to 22° in the laboratory frame. The differential cross section is defined by the following equation,

$$\left(\frac{d\sigma}{d\Omega}\right) = \frac{1}{N_{target}} \cdot \frac{1}{N_{beam} \cdot f_{K^+beam} \cdot f_{K^+decay} \cdot \epsilon_{K6}} \cdot \frac{1}{\epsilon_{LC} \cdot \epsilon_{TOF} \cdot f_{\pi^+decay} \cdot f_{\pi^+int}} \cdot \frac{1}{N_{\Theta^+} \cdot \epsilon_{SdcIn} \cdot \epsilon_{SdcOut} \cdot \epsilon_{Sks} \cdot \epsilon_{Sdc1} \cdot \epsilon_{vtx} \cdot d\Omega}, \quad (1)$$

where the f 's and ϵ 's represent the correction factors and efficiencies whose typical values are summarized in Table II.

The f_{K^+beam} represents the ratio of the number of K^+ 's which hit the LH₂ target to that of K^+ 's identified from the time-of-flight between BH1 and BH2. Because the horizontal size of the beam at the target region was comparable with the target size, part of the beam particles did not pass through the target. The f_{K^+beam} 's are estimated to be $84.5 \pm 3.5\%$ and $96.2 \pm 1.6\%$ for the 1st and 2nd runs, respectively, using data taken with a KBEAM trigger where there was no bias of scattered particles. Because the beam center was slightly shifted from the target center in the 1st run, the f_{K^+beam} in the 1st run was smaller than that in the 2nd run. The coefficient, f_{K^+decay} , represents the correction factor due to the decay in flight of the K^+ beam particles between BH2 and the LH₂ target. The f_{K^+decay} 's were estimated to be $96.7 \pm 0.1\%$ and $95.7 \pm 0.1\%$ for the 1st and 2nd runs, respectively. In the 2nd run, BH2 was moved to upstream in order to install BDC5. Therefore the f_{K^+decay} of the 2nd run was smaller than that of the 1st run.

The ϵ_{K6} represents the tracking efficiency for the in-

cident particles, estimated by the ratio of the number of events accepted as a good trajectory to that of good beam particles defined using the time-of-flight between BH1 and BH2 and the energy deposit at BH2. The ϵ_{K6} 's were obtained to be 95.3 ± 0.3 and 95.6 ± 0.3 for the 1st and 2nd runs, respectively.

The ϵ_{LC} and ϵ_{TOF} represent the efficiencies of LC and TOF counters, respectively. The LC and TOF were segmented horizontally into 14 and 15 segments, respectively. These efficiencies are estimated for each segment using data taken in the trigger condition without LC and TOF. The typical value of ϵ_{LC} was $95.5 \pm 0.2\%$. In order to obtain the cross section, the efficiency of the segment through which the outgoing π^+ passed was used. The typical value of the ϵ_{TOF} was almost 100%.

The coefficient, f_{π^+decay} , represents the correction factor due to the decay-in-flight of the π^+ . In the offline analysis, we required the hits of the LC and TOF corresponding to the trajectory obtained by the tracking routine using SDC3-4. From Monte Carlo simulations, we found that events where π^+ 's decayed after SDC4 could be analyzed as good events, because the angle of the μ^+ from the π^+ decay was less than 4° . Therefore the f_{π^+decay} was calculated event by event using the flight length from the vertex point to the exit of SDC4. The typical value of f_{π^+decay} was $85.2 \pm 0.2\%$. The coefficient, f_{π^+int} , represents the correction factor due to the interaction rate of π^+ in the materials of the target and the SKS spectrometer. The factor was calculated with the Monte Carlo simulation based on GEANT4. The value of f_{π^+int} was found to be $94 \pm 2\%$.

The coefficients, ϵ_{SdcIn} and ϵ_{SdcOut} , represent the efficiencies of the local tracking upstream and downstream of the SKS magnet. The ϵ_{SdcIn} was estimated from Monte Carlo simulations to be $87 \pm 1\%$. Typically there were multiple hits in SDC1 because it was designed to detect many charged particles at once. Therefore hits of SDC1 and SDC2 which did not originate from a single particle were connected in the tracking routine and finally rejected by the further analysis. The ϵ_{SdcOut} was estimated using the data of five beam-through runs where the π^+ beams of fixed momentum from 0.475 to 0.525 GeV/c were directly analyzed with the SKS spectrometer. The efficiency was constant for all horizontal positions of the outgoing particle. The ϵ_{SdcOut} was obtained to be $92.9 \pm 0.3\%$. The coefficient, ϵ_{SKS} , represents the efficiency of the Runge-Kutta tracking which calculates the trajectory of the outgoing particle by connecting local tracks. The ϵ_{SKS} was estimated by using scattered protons selected only using TOF and LC. The efficiency depended on the slope in the vertical plane (dy/dz) of the outgoing particle at the target. For small slope ($dy/dz \sim 0$), the ϵ_{SKS} was $95 \pm 0.7\%$. For large slope ($dy/dz \sim \pm 0.8$), the ϵ_{SKS} was $89 \pm 1\%$. The efficiency was corrected according to the slope of each trajectory.

The coefficient, ϵ_{Sdc1} , represents the efficiency of the SDC1 analysis described in the previous paragraph. The ϵ_{Sdc1} was obtained to be $69.4 \pm 3.7\%$.

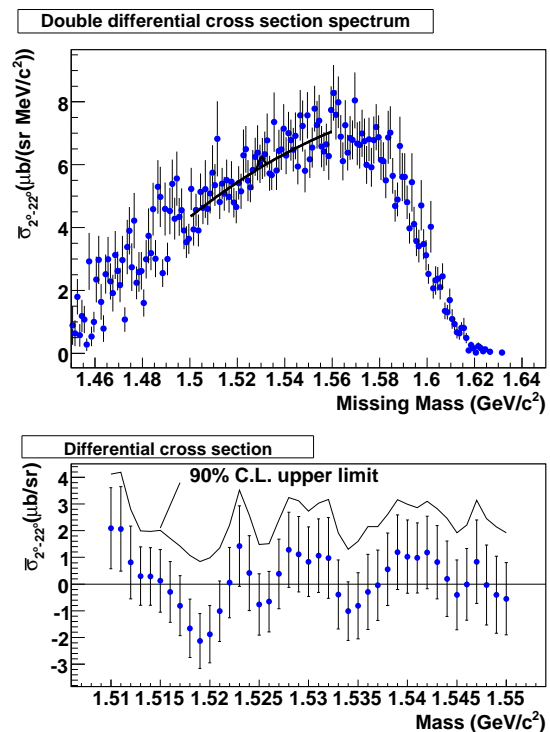


FIG. 9: Top figure: Double differential cross section of the $K^+p \rightarrow \pi^+X$ reaction averaged over 2° to 22° in the laboratory frame. This spectrum includes a contribution from the K^+ decay events which exist between the arrows in Fig. 7. In order to derive the upper limit of the differential cross section of the $K^+p \rightarrow \pi^+\Theta^+$ reaction, we fitted this spectrum with a background using a 2nd order polynomial function and a Gaussian peak with a fixed width of $2.4 \text{ MeV}/c^2$ (FWHM). Bottom figure: The upper limits of the differential cross section of the $K^+p \rightarrow \pi^+\Theta^+$ reaction averaged over 2° to 22° in the laboratory frame as a function of the mass of the Θ^+ . The data points show the value and the error of the differential cross section obtained from the area of the fitted Gaussian function. The line shows the 90% C.L. upper limit of the differential cross section.

The coefficient, ϵ_{vtx} , represents the efficiency of the vertex cut. In order to estimate this value, we used the vertex distribution of the (π^+, π^+) events, because the target image could be identified more precisely. The ϵ_{vtx} values are $85.2^{+2.9}_{-1.0}\%$ and $85.0^{+0.4}_{-0.9}\%$ for the 1st and 2nd runs, respectively. The coefficient ϵ_{Bdc5} represents the efficiency of the BDC5 analysis applied only in the 2nd run. This value was also estimated by using the (π^+, π^+) data from the ratio of the number of events within the target region in the vertex distribution with and without the BDC5 cut. The value of ϵ_{Bdc5} is $91.6 \pm 0.2\%$.

Because some of efficiencies depended on the trajectory of the particle, these efficiencies were calculated event by event. The differential cross section averaged over 2° to 22° in the laboratory frame was calculated using the following equation,

$$\bar{\sigma}_{2^\circ-22^\circ} = \int_{2^\circ}^{22^\circ} \left(\frac{d\sigma}{d\Omega} \right) d\Omega / \int_{2^\circ}^{22^\circ} d\Omega. \quad (2)$$

Fig. 9 shows the differential cross section versus missing mass which also shows no peak structure. This spectrum includes the contribution of K^+ decay events which exist between the arrows in Fig. 7. The error includes both of the statistical and systematic errors. We derived a 90 % C.L. upper limit of the differential cross section of the $K^+p \rightarrow \pi^+\Theta^+$ reaction. As shown in the top figure of Fig. 9, we fitted this spectrum with a background using a 2nd order polynomial function and a Gaussian peak with a width of 2.4 MeV/ c^2 (FWHM) which is the expected resolution for the Θ^+ . The differential cross section was calculated from the area of the Gaussian function. The bottom figure of Fig. 9 shows the values and the errors of the differential cross section as a function of the peak position. The solid line in the bottom figure of Fig. 9 shows the 90 % C.L. upper limit of the differential cross section considering that this distribution is based on Gaussian statistics. This 90 % C.L. upper limit is less than 3.5 $\mu\text{b/sr}$ for almost all mass region.

IV. DISCUSSION

The experimental results are now compared with theoretical calculations. A production mechanism based on both the present results of the $K^+p \rightarrow \pi^+\Theta^+$ reaction and the results of the $\pi^-p \rightarrow K^-\Theta^+$ reaction will be discussed.

In the $K^+p \rightarrow \pi^+\Theta^+$ reaction, it is possible to consider a t -channel process where K^{0*} is exchanged and a u -channel process where N^* is an intermediate state as shown in Fig. 10. Fig. 12 shows the differential cross

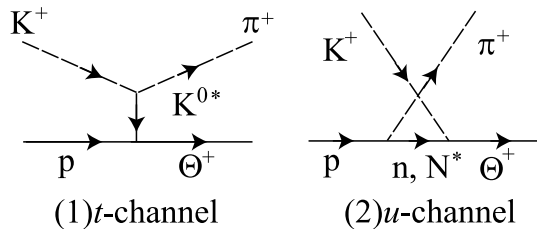


FIG. 10: Diagrams for the $K^+p \rightarrow \pi^+\Theta^+$ reaction.

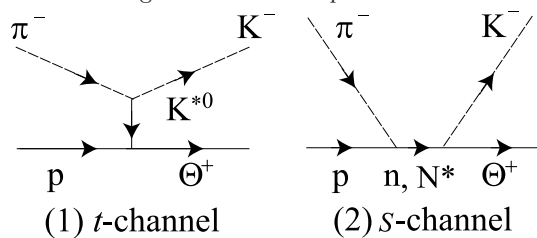


FIG. 11: Diagrams for the $\pi^-p \rightarrow K^-\Theta^+$ reaction.

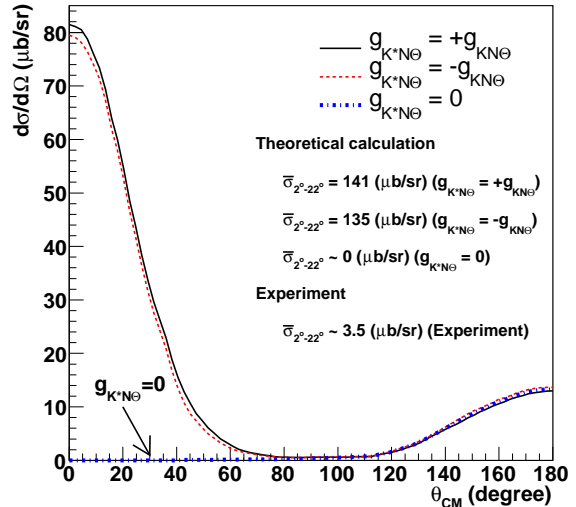


FIG. 12: Differential cross section calculated by Y. Oh *et al.* at $\sqrt{s}=2.4$ GeV (the present experiment was carried out at $\sqrt{s}=1.9$ GeV). This is the same as Fig. 3 (c) in Ref. [35]. The horizontal axis represents the scattering angle of the π^+ in the c.m. frame of K^+p system. The solid line is obtained with $g_{K^*N\Theta} = +g_{KN\Theta}$, the dashed line with $g_{K^*N\Theta} = -g_{KN\Theta}$, and the dot-dashed line with $g_{K^*N\Theta} = 0$. The differential cross sections averaged over 2° to 22° in the laboratory frame are also listed for each case.

section calculated by Y. Oh *et al.* using an effective interaction Lagrangian [35]. Their calculation is controlled by two coupling constants, $g_{KN\Theta}$ and $g_{K^*N\Theta}$. The coupling constant $g_{KN\Theta}$ is related to the decay width of the Θ^+ . They assumed that $g_{KN\Theta}$ was 1.0 which corresponds to a decay width of 1.03 MeV/ c^2 . On the other hand, there is no experimental information about $g_{K^*N\Theta}$. Therefore they calculated in three cases where $g_{K^*N\Theta} = 0$, $g_{K^*N\Theta} = g_{KN\Theta}$ and $g_{K^*N\Theta} = -g_{KN\Theta}$. If there is the t -channel process ($g_{K^*N\Theta} = \pm g_{KN\Theta}$), the differential cross section would have a forward peak distribution as shown by the solid and dashed lines in Fig. 12. The calculated differential cross section averaged over 2° to 22° in the laboratory frame ($\bar{\sigma}_{2^\circ-22^\circ}$) is about 140 $\mu\text{b/sr}$ in this case. The experimental upper limit of 3.5 $\mu\text{b/sr}$ is much smaller than this theoretical value. Therefore the t -channel process is excluded by the present results. On the other hand, if the t -channel process does not exist and only the u -channel process exists, the differential cross section shows a backward peak distribution as shown by the dot-dashed line in Fig. 12. In this case, the $\bar{\sigma}_{2^\circ-22^\circ}$ is almost 0 $\mu\text{b/sr}$. Our experiment is not sensitive enough to exclude the u -channel process.

The E522 collaboration reported an upper limit of the cross section of the $\pi^-p \rightarrow K^-\Theta^+$ reaction of 3.9 μb at the 90% confidence level assuming that the Θ^+ is produced isotropically in the center of mass system. In the $\pi^-p \rightarrow K^-\Theta^+$ reaction, the t -channel and s -channel pro-

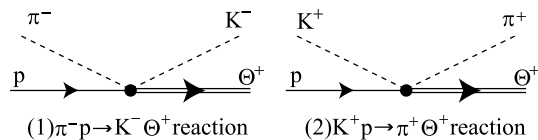


FIG. 13: Diagrams with two-meson coupling for the $\pi^-p \rightarrow K^-\Theta^+$ and $K^+p \rightarrow \pi^+\Theta^+$ reactions.

cesses are considered as shown in Fig. 11. The cross section is controlled by the same coupling constants, $g_{K^*N\Theta}$ and $g_{KN\Theta}$, which are used for the $K^+p \rightarrow \pi^+\Theta^+$ reaction. In order to explain the small cross section, the following two things are possible: 1) The coupling constant $g_{KN\Theta}$ is small; 2) Although the coupling constants $g_{K^*N\Theta}$ and $g_{KN\Theta}$ are sizable, the total cross section becomes small due to a destructive interference between two amplitudes of $g_{K^*N\Theta}$ and $g_{KN\Theta}$. From the result of the $K^+p \rightarrow \pi^+\Theta^+$ reaction, $g_{K^*N\Theta}$ is considered to be quite small. Therefore it is unlikely that the cross section is small due to the interference. If $g_{KN\Theta}$ is small, then the width of Θ^+ is quite narrow.

Hyodo and Hosaka studied the production mechanism taking into account the importance of two-meson couplings [45]. They calculated the production cross section of the $\pi^-p \rightarrow K^-\Theta^+$ and $K^+p \rightarrow \pi^+\Theta^+$ reactions for both $J^P = 1/2^+$ and $3/2^-$ using the Feynman diagrams shown in Fig. 13. They obtained the scalar and vector coupling constants of $\Theta K\pi N$, g^s and g^v , using flavor SU(3) symmetry and the decay width of the $N^*(1710) \rightarrow \pi\pi N$. Without a two-meson coupling, all of the amplitudes for the Θ^+ production are proportional to the $g_{KN\Theta}$ coupling, which is fixed by the supposed small decay width of the Θ^+ . However, even with an extremely narrow width of the Θ^+ , a sizable cross section can be obtained using the two-meson coupling determined from the decay width of $N^*(1710)$. These coupling constants have uncertainty due to the experimental uncertainties in the branching ratio. They restricted the coupling constants to be consistent with the upper limit of the cross section of the $\pi^-p \rightarrow K^-\Theta^+$ reaction. Moreover the relative phase between scalar and vector coupling constants could not be determined solely from the decay width of the $N^*(1710)$. This relative phase is quite important because it determines the interference term of these two amplitudes. If g_s and g_v have the same phase, the two amplitudes interfere constructively for the $\pi^-p \rightarrow K^-\Theta^+$ channel, while in the $K^+p \rightarrow \pi^+\Theta^+$ case it gives destructive interference. On the other hand, if g_s and g_v have the opposite phase, the situations for constructive and destructive interference reverse. Considering the small cross section obtained in the $\pi^-p \rightarrow K^-\Theta^+$ reaction, these data suggest the latter case. Then, the cross section of the $K^+p \rightarrow \pi^+\Theta^+$ reaction could be large. They calcu-

lated total cross sections of 2.5 mb and 110 μb in the cases of $J^P = 1/2^+$ and $3/2^-$, respectively. The $\bar{\sigma}_{2^\circ-22^\circ}$'s are $\sim 600 \mu\text{b/sr}$ and $\sim 50 \mu\text{b/sr}$ in each case. The experimental upper limit of 3.5 $\mu\text{b/sr}$ is much smaller than these calculations. If they take the same phase for g_s and g_v in order to explain the cross section of the $K^+p \rightarrow \pi^+\Theta^+$ reaction, the cross section of the $\pi^-p \rightarrow K^-\Theta^+$ becomes large due to the constructive interference, which is inconsistent with the experimental result. Therefore this model can not explain both of the experimental results simultaneously.

In summary, we have searched for the Θ^+ via the $K^+p \rightarrow \pi^+X$ reaction using a 1.2 GeV/c K^+ beam at the K6 beam line of the KEK-PS 12 GeV Proton Synchrotron. In the missing mass spectrum of the $K^+p \rightarrow \pi^+X$ reaction, no clear peak structure was observed. A 90 % C.L. upper limit of the differential cross section, averaged over 2° to 22° in the laboratory frame of the $K^+p \rightarrow \pi^+\Theta^+$ reaction, is obtained at 3.5 $\mu\text{b/sr}$. From the present experiment and the experiment by the E522 collaboration, it is found that both of the production cross sections from the $\pi^-p \rightarrow K^-\Theta^+$ and $K^+p \rightarrow \pi^+\Theta^+$ reactions are small. From the small differential cross section at the forward angles of the $K^+p \rightarrow \pi^+\Theta^+$ reaction, the t -channel process, where a K^{0*} is exchanged, is excluded. Therefore the small cross section of the $\pi^-p \rightarrow K^-\Theta^+$ reaction cannot be explained by the destructive interference between two amplitudes due to the couplings $g_{KN\Theta}$ and $g_{K^*N\Theta}$. In order to explain the small cross section, the coupling constant $g_{KN\Theta}$ must be small. The model by Hyodo and Hosaka which explains the result of the $\pi^-p \rightarrow K^-\Theta^+$ reaction also cannot explain the present result.

V. ACKNOWLEDGMENTS

We would like to express our thanks to staffs of KEK PS and beam channel group for their support to provide beam with the excellent condition during the experiment. We would like to thanks to RIKEN Radiation Laboratory for the usage of RIKEN-CCJ computer system. Some of the authors (K. M.) and (S. D.) thank to the Japan Society for the Promotion of Science (JSPS) for support. One author (K.H.) thanks the National Science Foundation for support. This work was supported by the Grant-in-Aid for the 21st Century COE "Center for Diversity and Universality in Physics" from the Ministry of Ministry of Education, Culture, Science and Technology (MEXT) of Japan. This work was supported by the Grant-in-Aid for Specially Promoted Research (No.15001001) from the Ministry of Education, Culture, Science and Technology, Japan.

[1] T. Nakano *et al.*, Phys. Rev. Lett. **91**, 012002 (2003).

[2] K.H. Hicks, Prog. Nucl. Part. Phys. **55**, 647 (2005).

- [3] K. Goeke, H.-C. Kim, M. Praszalowicz and G.-S. Yang, Prog. Nucl. Part. Phys. **55**, 350 (2005).
- [4] DIANA Collaboration, V.V. Barmin *et al.*, Phys. Atom. Nucl. **66**, 1715 (2003).
- [5] CLAS Collaboration, S. Stepanyan *et al.*, Phys. Rev. Lett. **91**, 252001 (2003).
- [6] SAPHIR Collaboration, J. Barth *et al.*, Phys. Lett. B **572**, 127 (2003).
- [7] CLAS Collaboration, V. Kubarovsky *et al.*, Phys. Rev. Lett. **92**, 032001 (2004).
- [8] A. E. Asratyan, A.G. Dolgolenko and M.A. Kubantsev, Phys. Atom. Nucl. **67**, 682 (2004).
- [9] HERMES Collaboration, A. Airapetian *et al.*, Phys. Lett. B **585**, 213 (2004).
- [10] ZEUS Collaboration, S. Chekanov *et al.*, Phys. Lett. B **591**, 7 (2004).
- [11] COSY-TOF Collaboration, M. Abdel-Bary *et al.*, Phys. Lett. B **595**, 127 (2004).
- [12] SVD Collaboration, A. Aleev *et al.*, arXiv:hep-ex/0401024.
- [13] P.Zh. Aslanyan *et al.*, arXiv:hep-ex/0403044.
- [14] Hyper-CP Collaboration, M.J. Longo *et al.*, Phys. Rev. D **70**, 111101(R) (2004).
- [15] HERA-B Collaboration, I. Abt *et al.*, Phys. Rev. Lett. **93**, 212003 (2004).
- [16] ALEPH Collaboration, S. Schael *et al.*, Phys. Lett. B **599**, 1 (2004).
- [17] BES Collaboration, J.Z. Bai *et al.*, Phys. Rev. D **70**, 012004 (2004).
- [18] BABAR Collaboration, B. Aubert *et al.*, hep-ex/0502004.
- [19] CDF Collaboration, D.O. Litvintsev *et al.*, Nucl. Phys. B (Proc. Suppl.) **142**, 374 (2005).
- [20] SPHINX Collaboration, Yu.M. Antipov *et al.*, Eur. Phys. J. **A21**, 455 (2004).
- [21] PHENIX Collaboration, C. Pinkenburg *et al.*, J. Phys. G : Nucl. Part. Phys. **30**:S1201 (2004).
- [22] CLAS Collaboration, M. Battaglieri *et al.*, Phys. Rev. Lett. **96** 042001 (2006) .
- [23] CLAS Collaboration, B. McKinnon *et al.*, Phys. Rev. Lett. **96** 212001 (2006) .
- [24] COSY-TOF Collaboration, M. Abdel-Bary *et al.*, Phys. Lett. B **649**, 252 (2007).
- [25] T. Nakano *et al.*, J. Phys. G: Nucl. Part. Phys. **32** S77 (2006).
- [26] DIANA Collaboration, V.V. Barmin *et al.*, hep-ex/0603017 .
- [27] R.A. Arndt, I.I. Strakovsky, and R.L. Workman, Phys. Rev. C **68**, 042201(R) (2003).
- [28] R.N. Cahn and G.H. Trilling, Phys. Rev. D **69**, 011501(R) (2004).
- [29] D. Diakonov, V. Petrov, M. Polyakov, Z. Phys. A **359**, 305 (1997).
- [30] R. Jaffe, F. Wilczek, Phys. Rev. Lett. **91**, 232003 (2003).
- [31] M. Karliner, H.J. Lipkin, Phys. Lett. B **575**, 249 (2003).
- [32] T. Kishimoto and T. Sato, hep-ex/0312003.
- [33] Y. Kanada-En'yo, O. Morisatsu and T. Nishikawa, hep-ph/0410221.
- [34] E. Hiyama, H. Suganuma and M. Kaminura, arXiv:0707.4044.
- [35] Y. Oh, H. Kim, and S.H. Lee , Phys. Rev. D **69**, 074016 (2004).
- [36] KEK-PS E522 Collaboration, K. Miwa *et al.*, Phys. Lett. B **635**, 72 (2006).
- [37] T. Fukuda *et al.*, Nucl. Instr. Meth. A **361**, 485 (1995).
- [38] H. Hotchi *et al.*, Phys. Rev. C **64**, 044302 (2001).
- [39] O. Hashimoto, H. Tamura, Prog. Nucl. Part. Phys. **57**, 564 (2006).
- [40] R.W. Bland *et al.*, Nucl. Phys. B **13**, 595 (1969).
- [41] J. Myrheim and L. Bugge, Nucl. Instrum. Methods. **160** (1979) 43.
- [42] W. Liu and C.M. Ko , Phys. Rev. C **68**, 045203 (2003).
- [43] Y. Oh, H. Kim, and S.H. Lee , Phys. Rev. D **69**, 014009 (2004).
- [44] T. Hyodo, A. Hosaka, and E. Oset, Phys. Lett. B **579**, 290 (2004).
- [45] T. Hyodo, and A. Hosaka, Phys. Rev. C **72**, 055202 (2005).